

Sputtering Growth of Nitrogen-doped Ga₂O₃ Films and Applications of Photodetectors

Sufen Wei,^{1*} Qianqian Shi,¹ Yi Liu,¹ and Cheng-Fu Yang^{2,3**}

¹School of Ocean Information Engineering, Jimei University, Xiamen 361021, China

²Department of Chemical and Materials Engineering, National University of Kaohsiung, Kaohsiung 811, Taiwan

³Department of Aeronautical Engineering, Chaoyang University of Technology, Taichung 413, Taiwan

(Received January 3, 2024; accepted May 2, 2024)

Keywords: gallium oxide, magnetron sputtering, nitrogen-doped Ga₂O₃, near-UV photodetector

Thin-film Ga₂O₃-based solar- and visible-blind photodetectors (PDs) stand at the forefront of future applications, with their performance closely tied to film quality. Employing radio frequency magnetron sputtering, we deposited an intrinsic Ga₂O₃ thin film onto a double-throw (0001) sapphire substrate at a substrate temperature of 500 °C for 10 min. Subsequently, using the intrinsic Ga₂O₃ thin film as the substrate and maintaining constant process parameters, including background vacuum, working pressure, growth temperature, sputtering power, and duration, we introduced N₂ at various flow rates (0, 5, 10, 15, 20, and 25 sccm) for the reactive sputtering growth of nitrogen-doped amorphous Ga₂O₃ thin films. Field emission scanning electron microscopy (FESEM), atomic force microscopy (AFM), X-ray photoelectron spectroscopy (XPS), X-ray diffraction (XRD), UV–Vis spectrophotometry, and Hall effect measurements were utilized to probe the impact of N₂ flow rate on the growth rate, surface morphology, elemental composition, crystallization quality, and optical characteristics, and electrical properties of the Ga₂O₃ thin films. With increasing N₂ flow rate, the films exhibited a notable redshift of the absorption edge, accompanied by a decrease in optical band gap. Hall effect measurements confirmed the stable p-type conductivity of the nitrogen-doped Ga₂O₃ thin films. Subsequently, metal-semiconductor-metal-type PDs were fabricated using the nitrogen-doped Ga₂O₃ thin films. These PDs demonstrated heightened sensitivity to 365 nm near-UV light, boasting a remarkable response of 1.32×10^2 A/W and a high response speed of 0.028/0.17 s.

1. Introduction

Gallium oxide (Ga₂O₃) has emerged as a crucial material owing to its ultrawide bandgap (energy gap of approximately 4.9 eV) and transparent semiconducting properties.^(1,2) This versatile compound finds applications in various cutting-edge technologies such as next-generation power electronic devices,^(3–5) photodetectors (PDs),^(6–8) LEDs,^(2,9) photocatalysts,⁽¹⁰⁾ gas sensors,⁽¹¹⁾ solar cells,⁽¹²⁾ and phosphors.⁽¹³⁾ The bulk growth of Ga₂O₃ currently involves the

*Corresponding author: e-mail: weisufen@jmu.edu.cn

**Corresponding author: e-mail: cfyang@nuk.edu.tw

<https://doi.org/10.18494/SAM4890>

production of 2-inch-diameter crystal cylinders by the Czochralski method⁽¹⁴⁾ and 4-inch-diameter crystal slabs by the Edge-defined Film-fed Growth method (EFG).⁽¹⁵⁾ Additionally, various epitaxial techniques, including metal-organic chemical vapor deposition^(16,17) and molecular beam epitaxy,⁽¹⁸⁾ have been reported for the high-quality growth of Ga₂O₃.⁽¹⁹⁾ In contrast, RF magnetron sputtering presents a distinct approach that does not rely on complex precursor molecular reactions. By utilizing a Ga₂O₃ ceramic target and argon gas, this method allows electrons to gain energy from a high-frequency electric field, leading to collisions with argon atoms and the generation of plasma. This plasma transports material from the Ga₂O₃ ceramic target to the substrate. RF magnetron sputtering is a well-established, environmentally friendly, and cost-effective technology, making it highly suitable for the efficient preparation of large-area Ga₂O₃ thin films.^(20–22)

The structural quality of Ga₂O₃ thin films with a high carrier concentration plays a crucial role in advancing device development and applications. Presently, controllable n-type Ga₂O₃ thin films have been achieved through intentional doping with elements such as Si, Ge, Sn, Mg, and Fe, resulting in electron concentrations ranging from 10¹⁶ to 10²⁰ cm⁻³.^(1,2) However, achieving effective p-type conductivity in Ga₂O₃ requires further exploration in appropriate acceptor doping. Nitrogen (N) emerges as a promising candidate for p-type doping in Ga₂O₃.^(1,2) N, with an atomic radius close to that of O but one fewer valence electron and a higher energy 2p orbital than O, introduces shallow acceptor impurity energy levels above the valence band upon doping. Successful experimental evidence has been demonstrated for p-type N doping in Ga₂O₃ through the high-temperature thermal oxidization of GaN in O₂⁽²³⁾ or N₂O⁽²⁴⁾ atmosphere above 1100 °C. A high-sensitivity solar-blind-UV PD has been fabricated using p-type Ga₂O₃ thin films doped with N₂O by thermal oxidization.⁽²⁵⁾ In this study, the RF magnetron sputtering method was employed to deposit nitrogen-doped Ga₂O₃ thin films. Hall measurements were conducted to ascertain charge carrier type, concentration, mobility, and resistivity. The effects of N₂ flow rate on nitrogen incorporation and the bandgap were also analyzed. Metal-semiconductor-metal (MSM)-type PDs based on nitrogen-doped Ga₂O₃ thin films were subjected to time-dependent photoresponse assessments under 254 and 365 nm UV lights to evaluate the performance of the nitrogen-doped Ga₂O₃ thin films.

2. Medical Image Asymmetry Calculation Model

A 60-mm-diameter high-purity (4N) gallium oxide ceramic target and double-sided polished (0001) sapphire substrates (Φ50.8 mm × 430 μm) were employed in the experiment. The sapphire substrates underwent a cleaning process involving sequential immersions in acetone and alcohol for 15 min within an ultrasonic cleaning machine. Subsequently, they were rinsed in deionized water and dried using nitrogen. The gallium oxide ceramic target was positioned on the sputter gun, maintaining a distance of 8 (±2) cm from the substrate. Initially, utilizing RF magnetron sputtering, we grew an undoped (intrinsic) Ga₂O₃ thin film on the (0001) sapphire substrate at a substrate temperature of 500 °C for 10 min. In this phase, a mixture of high-purity (≥99.999%) argon (39 sccm) and O₂ (1 sccm) was utilized as the working gas, achieving an oxygen content of 2.5%. The background vacuum in the sputtering chamber was maintained below 4.0 × 10⁻⁴ Pa,

the working pressure during sputtering was set to 0.8 Pa, and the sputtering duration was 10 min at a power of 200 W.

Subsequently, utilizing the grown intrinsic Ga_2O_3 as the substrate, we maintained the process parameters, namely, background vacuum, working pressure, growth temperature, sputtering power, and sputtering duration, without changes. We introduced N_2 at different flow rates (0, 5, 10, 15, 20, and 25 sccm) for reactive sputtering, facilitating the generation of nitrogen-doped Ga_2O_3 thin films. The detailed parameters are summarized in Table 1, and a schematic diagram illustrating the sputtering growth of nitrogen-doped Ga_2O_3 thin films is presented in Fig. 1. To investigate the chemical characteristics of the Ga_2O_3 thin film surface, X-ray photoelectron spectroscopy (XPS) was employed, utilizing a ThermoFisher ESCALAB Xi+ instrument. Before the XPS measurement, a 15 kV applied voltage accelerated the Ar ion beam, with a sputtering rate of 0.16 nm s^{-1} for 30 s, effectively removing surface contamination from the samples. For an in-depth examination of the crystalline structure of the sputtering-grown nitrogen-doped Ga_2O_3 thin films, X-ray diffraction (XRD) analysis was conducted using a Malvern Panalytical EMPYREAN SERIES 3 instrument. The XRD analysis utilized a $\text{Cu K}\alpha$ ($\lambda = 1.54 \text{ \AA}$) X-ray source, covering the 2-theta range of $10\text{--}80^\circ$.

Atomic force microscopy (AFM, Oxford Instruments Asylum Research Cypher S) was utilized to examine the surface morphologies of the samples. The cross-sectional morphologies

Table 1
Parameters of the nitrogen doping by RF magnetron sputtering.

| Parameter | Value |
|---|----------------------------------|
| Target | Ga_2O_3 (99.99%) |
| Back pressure (Pa) | 4.0×10^{-4} |
| Work pressure (Pa) | 1.0×10^0 |
| RF power (W) | 200 |
| Sputtering time (min) | 20 |
| Target–substrate distance (cm) | 8 |
| Ar flow rate (sccm) | 39 |
| N_2 flow rate (sccm) | 0, 5, 10, 15, 20, 25 |
| Sputtering temperature ($^\circ\text{C}$) | 500 |

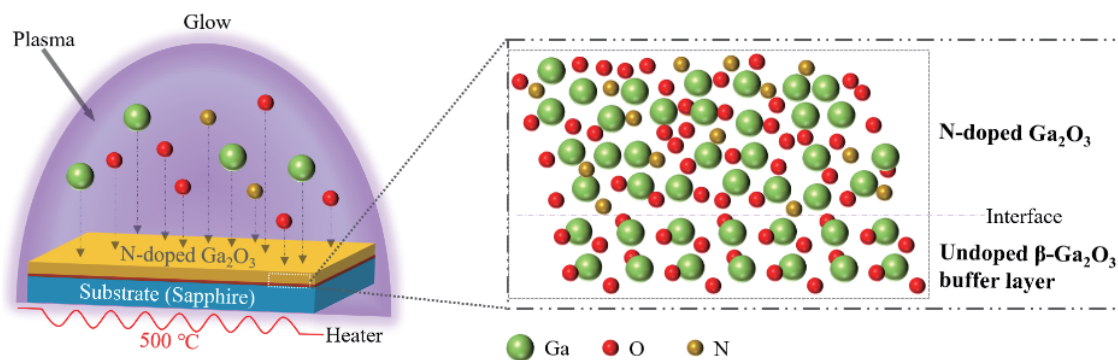


Fig. 1. (Color online) Schematic diagram of sputtering growth of nitrogen-doped Ga_2O_3 thin films.

were analyzed through field emission scanning electron microscopy (FESEM, Carl Zeiss/GeminiSEM300). UV-Vis spectrophotometry (U-3900H, Hitachi, Japan) was employed to measure the transmittance and absorption spectrum of the films. For the precise measurement of electrical properties, indium electrodes were sputtered, followed by rapid thermal annealing at 600 °C for 60 s to establish a reliable ohmic contact. Subsequently, temperature- and magnetic-field-dependent Van der Pauw Hall effect measurements were conducted (PPMS DynaCool-9) to analyze the electrical properties of the Ga₂O₃ thin films. PDs, based on nitrogen-doped Ga₂O₃ thin films with an MSM-type structure, were fabricated by sputtering interdigital Al electrodes on the films using a shadow mask and DC magnetron sputtering. The time-dependent photoresponse of the nitrogen-doped Ga₂O₃ thin-film-based PDs was measured at a fixed voltage of 5 V using a Keithley 4200A-SCS, with 254 and 365 nm UV lamps serving as UV light sources. Figure 2(a) shows the physical image of the PDs, whereas Fig. 2(b) shows the PDs' image captured using an RX50M high-power metallographic microscope. The thickness of the Al electrode was 200 nm.

3. Results and Discussion

The thicknesses of the nitrogen-doped Ga₂O₃ thin films were measured using FESEM. The thicknesses of the nitrogen-doped Ga₂O₃ thin films grown at N₂ flow rates of 0, 5, 10, 15, 20, and 25 sccm were found to be 212, 312, 385, 413, 458, and 447 nm, respectively. There was a significant increase in thickness, with the maximum value observed at a N₂ flow rate of 20 sccm. The growth rates were determined by dividing the thickness by the sputtering time, resulting in rates of 10.6, 15.6, 19.25, 20.65, 22.9, and 22.35 nm/min, respectively. Figure 3(a) shows the trend of the growth rate for nitrogen-doped Ga₂O₃ thin films at different N₂ flow rates. As the N₂ flow rate increased from 0 to 20 sccm, the growth rate of the thin films continued to increase within this range. Upon reaching a N₂ flow rate of 20 sccm, a saturation point in the growth rate was observed. This can be attributed to the fact that the introduced N₂ served as the reaction gas, and a higher amount led to increased participation in the reaction, resulting in thicker films and an improved growth rate. As the N₂ flow rate continued to increase to 25 sccm, a slight decrease in growth rate was noted, possibly due to the higher proportion of

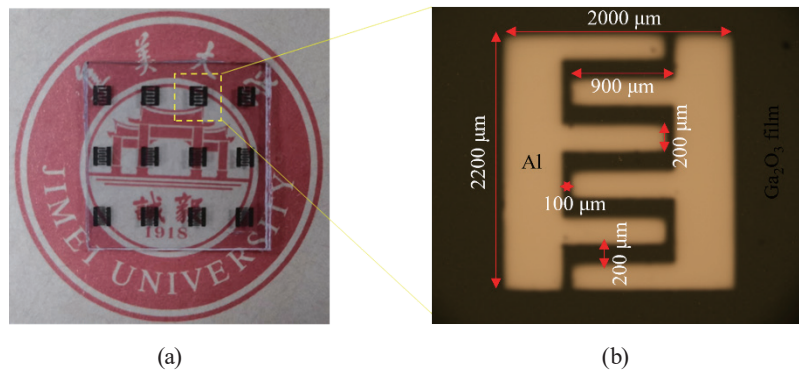


Fig. 2. (Color online) (a) Physical image of MSM-type Ga₂O₃-based PDs; (b) optical image showing device structure.

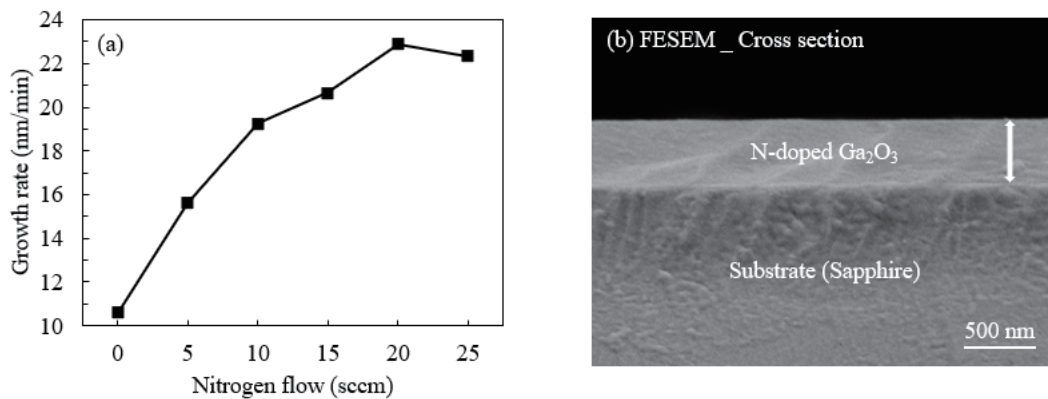


Fig. 3. (a) The nitrogen-doped Ga₂O₃ thin film's growth rate changes with the N₂ flow rate. (b) FESEM cross-sectional topography.

N₂ causing more N particles to attach to the surface of the target, thereby impacting the sputtering growth rate. Figure 3(b) shows the cross-sectional morphology of the thin film at a N₂ flow rate of 25 sccm, clearly distinguishing the substrate from the epitaxial thin film.

AFM was employed to assess the surface topography and root-mean-square (RMS) surface roughness of the nitrogen-doped Ga₂O₃ thin films. The 3D surface topography of samples at a scanning area of 4 μm² is depicted in Figs. 4(a)–4(f). According to the AFM results, as the N₂ flow rate increased from 0 to 25 sccm, the RMS values of the thin film samples were 16.5, 7.95, 7.61, 4.91, 3.85, and 25.5 nm. The thin film exhibited a decreasing trend in roughness within the range of 0–20 sccm, with the lowest roughness observed at 20 sccm, indicating the smoothest film surface. However, as the N₂ flow rate continued to increase to 25 sccm, the film's roughness increased to 25.5 nm. This was attributed to the emergence of island-shaped particles with irregular sizes, resulting in films with an amorphous structure and numerous defects. The AFM results underscore the effect of the N₂ flow rate on the thin film's roughness.

Figure 5(a) shows the XPS survey spectra of the Ga-related (3s, 3p, 3d, 2p), O-related (1s), N, Ga LMM, and O KLL of the RF-sputtered nitrogen-doped Ga₂O₃ thin films at different N₂ flow rates. The XPS data were calibrated using the standard C 1s peak located at a binding energy of 284.8 eV. The O 1s spectra were then differentiated and fitted with two peaks, as illustrated in Figs. 5(b)–5(g). The O 1s spectral peak was decomposed into a lattice oxygen peak and a non-lattice oxygen peak. In particular, the binding energy of the lattice oxygen peak, ranging between 530 and 531 eV, was attributed to the Ga–O bond, representing the O²⁻ ion in the lattice. The binding energy of the non-lattice oxygen peak, found between 531.5 and 532.5 eV, primarily originated from O²⁻ ions in the oxygen defect region, as well as the chemisorption of carboxyl groups and carbonates, indicating the absence of O in the films. The peak area ratios of the non-lattice oxygen to the sum of lattice oxygen and non-lattice oxygen were 4.01%, 9.89%, and 9.91%, at N₂ flow rates of 0, 5, and 10 sccm. However, as the N₂ flow rate increased to 15 sccm, the non-lattice oxygen peak exhibited a notable enhancement, reaching its maximum intensity at 25 sccm. The area ratio of the two peaks was calculated to determine the specific proportion, providing a measure of the relative proportion of O-related defects in the nitrogen-doped Ga₂O₃ thin films.

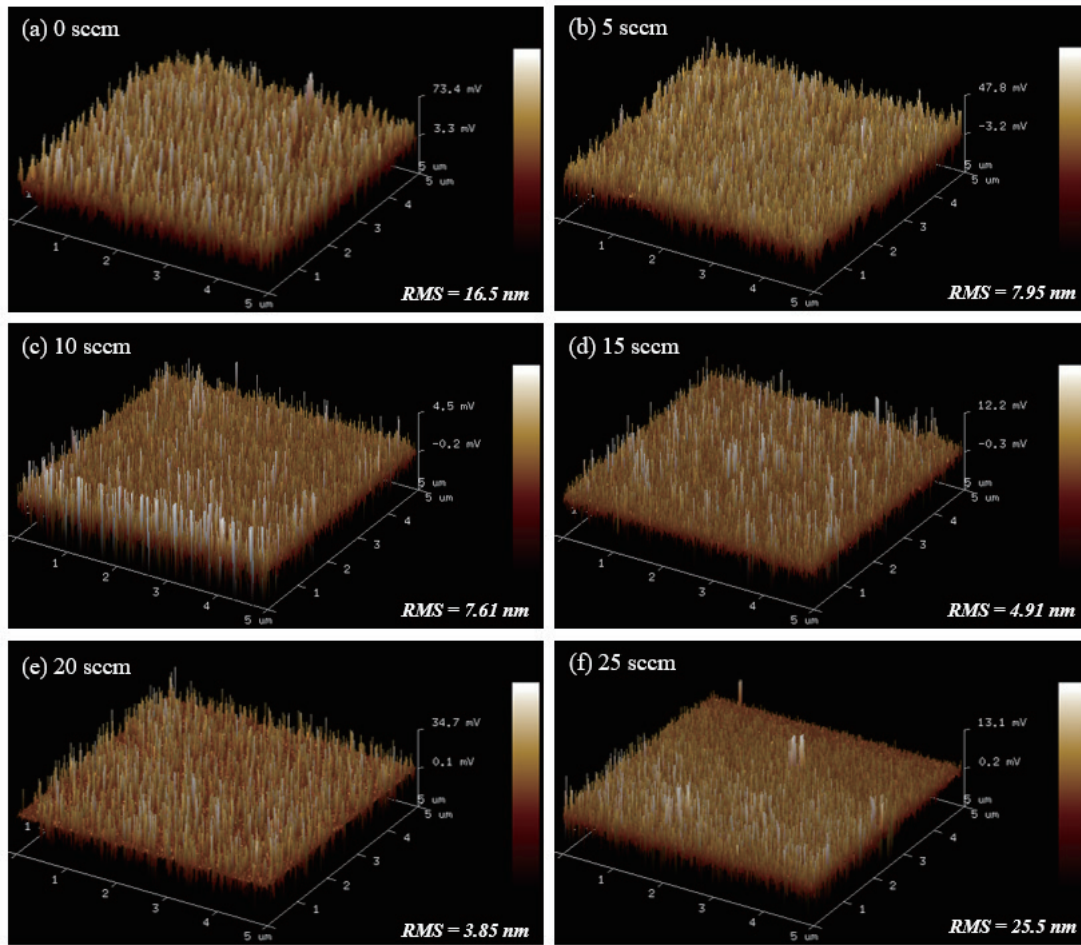


Fig. 4. (Color online) AFM surface 3D morphology of nitrogen-doped Ga_2O_3 thin films under different N_2 flow rates: (a) 0, (b) 5, (c) 10, (d) 15, (e) 20, and (f) 25 sccm.

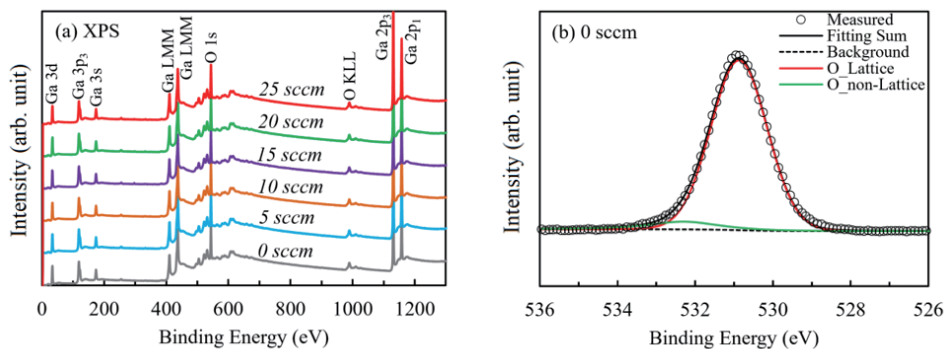


Fig. 5. (Color online) XPS spectra of nitrogen-doped Ga_2O_3 thin films at different N_2 flow rates: (a) survey scans of XPS spectra, (b)–(g) O 1s core energy level peak spectra under different N_2 flow rates, and (h) percentage change of lattice oxygen to non-lattice oxygen.

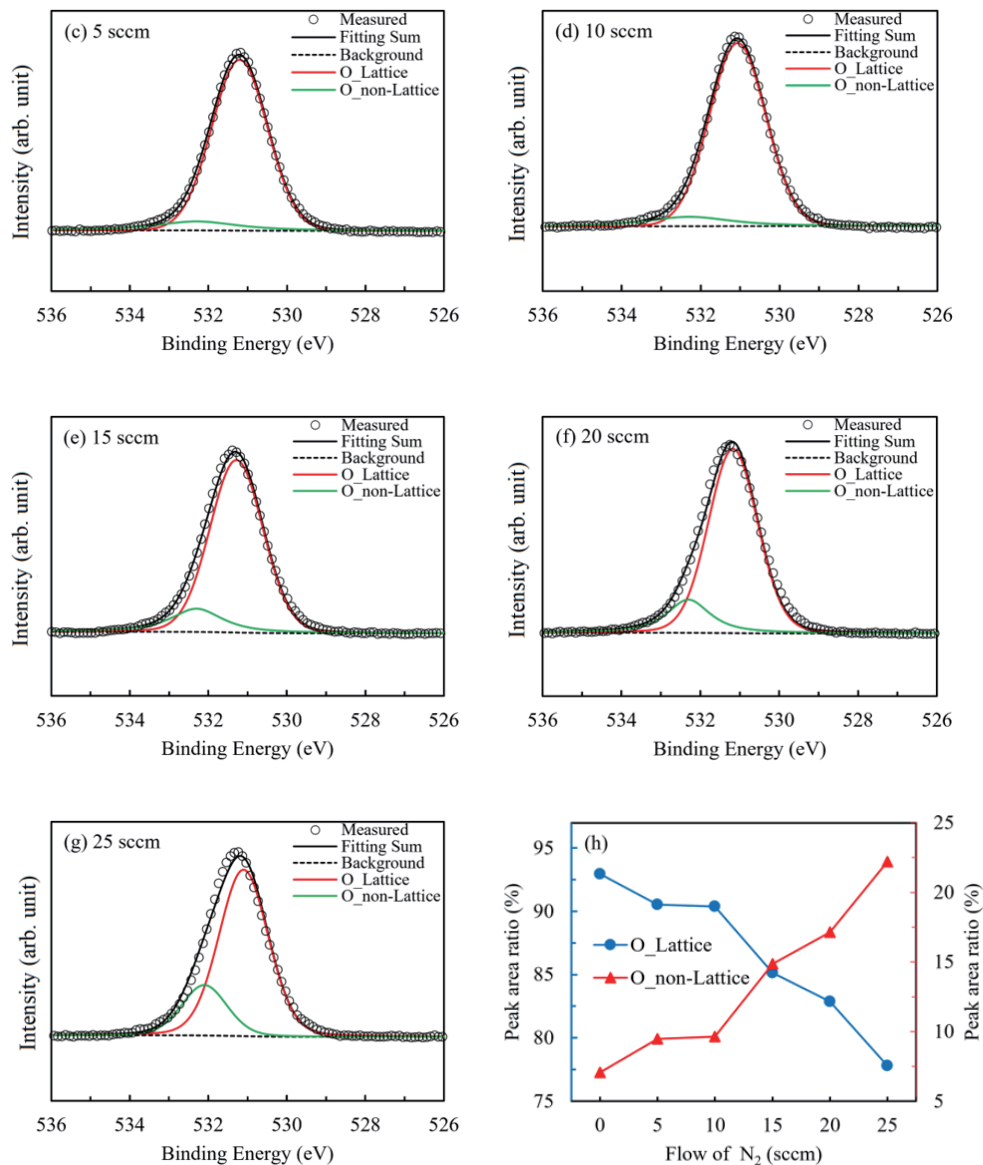


Fig. 5. (Color online) (Continued) XPS spectra of nitrogen-doped Ga₂O₃ thin films at different N₂ flow rates: (a) survey scans of XPS spectra, (b)–(g) O 1s core energy level peak spectra under different N₂ flow rates, and (h) percentage change of lattice oxygen to non-lattice oxygen.

The trend of variation under different N₂ flow rates is shown in Fig. 5(h). The specific proportions of non-lattice oxygen corresponding to N₂ flow rates of 0, 5, 10, 15, 20, and 25 sccm were 7.06, 9.48, 9.63, 14.86, 17.41, and 22.21%, respectively. It is evident that, as the N₂ flow rate increased, the area ratio of non-lattice oxygen peaks exhibited a continuous growth trend, with a gradual increase in the range of 0 to 10 sccm. However, at a N₂ flow rate of 15 sccm, the proportion of non-lattice oxygen began to increase rapidly. In contrast, lattice oxygen showed the opposite trend. Under specific pressure conditions, an increase in N₂ flow rate created a N-rich

preparation environment, reducing the formation energy of external natural oxygen defects, leading to an increase in the amount of internal defects in Ga_2O_3 thin films. Additionally, owing to the doping of N atoms into Ga_2O_3 thin films, some Ga–O bonds were replaced by Ga–N bonds, resulting in a decrease in the proportion of the lattice oxygen peak area. The substrate growth temperature being set at 500 °C may contribute to more oxygen-related defects. Elevated temperatures heightened the vibrational activity of lattice atoms, potentially causing oxygen atoms to detach from their bound states and migrate into an anaerobic environment. Subsequently, this process may result in the creation of oxygen vacancies.

The XRD patterns of the RF-sputtered nitrogen-doped Ga_2O_3 thin films were analyzed to assess the formation of the Ga_2O_3 phase at various N_2 flow rates, and the results are shown in Fig. 6. The XRD results were compared with standard powder diffraction files from COD-2004987: PDF# 43-1012 for $\beta\text{-Ga}_2\text{O}_3$ and PDF# 50-1496 for sapphire. To eliminate the effect of the intrinsic Ga_2O_3 substrate on the XRD patterns, nitrogen-doped Ga_2O_3 thin films were resputtered directly onto the sapphire substrate using the same parameters. These samples were specifically prepared for XRD testing only. In Fig. 6, it is evident that, apart from the diffraction peak of the sapphire substrate, only the $(\bar{4}02)$ crystal plane diffraction peak belonging to $\beta\text{-Ga}_2\text{O}_3$ appeared near 38° at N_2 flow rates of 0 and 5 sccm. Even at a N_2 flow rate of 5 sccm, the diffraction peak intensity of the $(\bar{4}02)$ crystal plane belonging to $\beta\text{-Ga}_2\text{O}_3$ had already weakened significantly, indicating that the introduction of reactive N_2 gas disrupted the ordered arrangement of Ga and O, reducing the crystallization performance of the thin films. At N_2 flow rates ranging from 10 to 25 sccm, no diffraction peaks corresponding to gallium oxide were detected, indicating that the Ga_2O_3 thin films grown within this N_2 flow rate range were amorphous. Overall, the trend suggests that with the increase in N_2 flow rate and a higher concentration of N atoms, the atomic arrangement of the nitrogen-doped Ga_2O_3 thin films became increasingly disordered, resulting in a decrease in crystal quality.

Figure 7(a) shows the UV–Vis transmission spectrum of the nitrogen-doped Ga_2O_3 thin films. The blank sapphire substrate exhibited an average transmission of about 85%, and all the thin films showed high transmission in the visible wavelength region, surpassing 80%. This

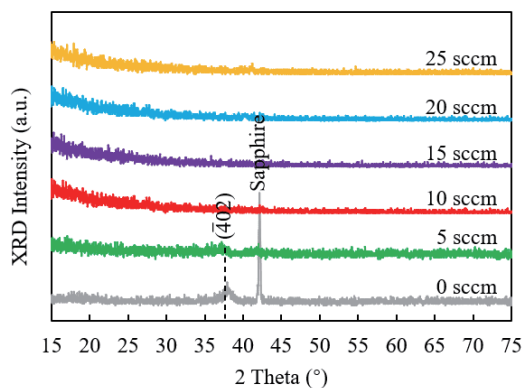


Fig. 6. (Color online) XRD patterns of the nitrogen-doped Ga_2O_3 thin films at different N_2 flow rates.

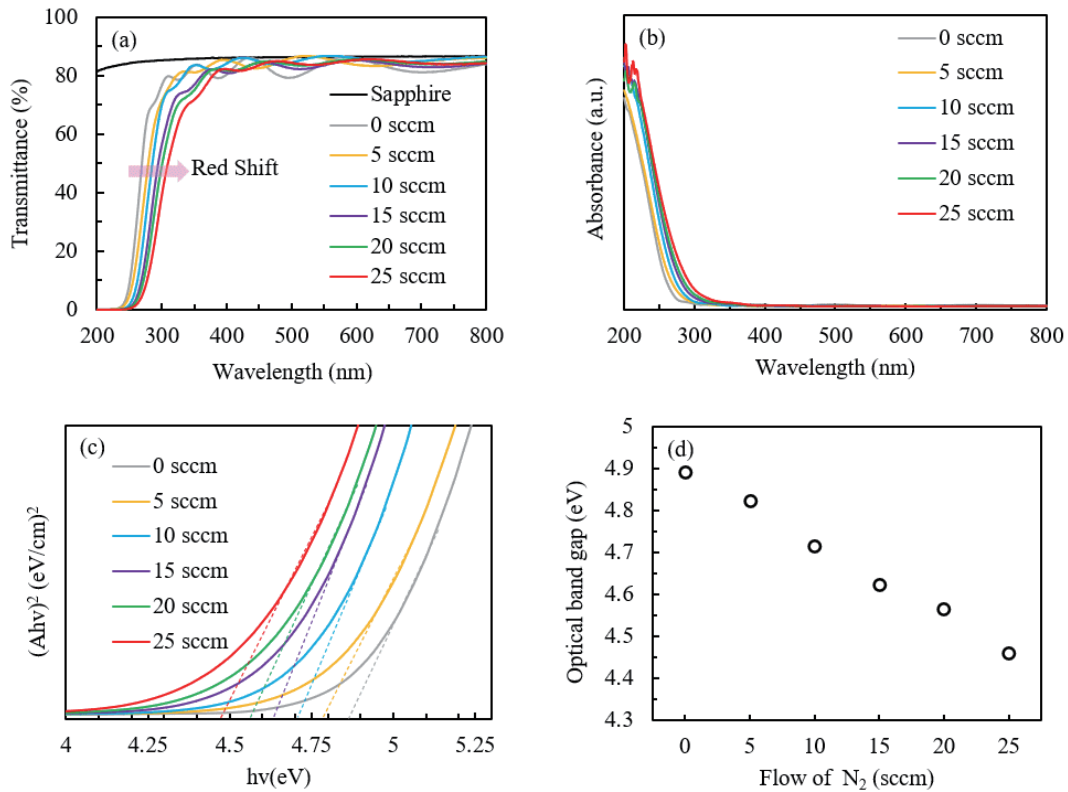


Fig. 7. (Color online) Optical properties of the nitrogen-doped Ga_2O_3 thin films at different N_2 flow rates: (a) light transmission spectrum, (b) light absorption spectrum, (c) $h\nu - (Ah\nu)^2$ relationship curve, and (d) trend chart of bandgap width variation.

indicates that the average light transmission of the nitrogen-doped Ga_2O_3 thin films in the visible region had a weak dependence on the N_2 flow rate. The disordered wave shape observed in the transmittance in the visible light region is attributed to the resonance phenomenon caused by the thickness of the films. Additionally, Fig. 7(a) suggests that the undoped Ga_2O_3 thin film grown at 0 sccm exhibited a clear absorption edge at a wavelength of ~ 275 nm (UV-C). With an increase in N_2 flow rate, the UV absorption cutover of the film gradually shifted to longer wavelengths, resulting in a redshift phenomenon. The redshift indicates that, as nitrogen replaces the oxygen lattice site, Ga–N bonds are formed, leading to a decrease in the band gap of the film. At a N_2 flow rate of 25 sccm, the absorption edge shifted to the near-UV region (UV-A). Figure 7(b) shows the absorption spectrum of the film, corresponding to the transmission spectrum, and the change trend is consistent. On the basis of the absorption spectrum, the band gap (E_g) of the film was calculated and is plotted in Figs. 7(c) and 7(d). It was observed that E_g decreased with the increase in N_2 flow rate.

The Hall effect measurements of the conductivity type, Hall carrier concentration (N_e , N_p), mobility (μ), and resistivity (ρ) of the nitrogen-doped Ga_2O_3 thin films grown by RF sputtering at different N_2 flow rates are summarized in Table 2. It can be observed from the table that the

Table 2

Hall effect measurements for the nitrogen-doped Ga₂O₃ thin films at different N₂ flow rates.

| N ₂ flow rate (sccm) | Type | N_e, N_p (cm ⁻³) | μ (cm ² /V·s) | ρ (Ω ·cm) |
|---------------------------------|----------|--------------------------------|------------------------------|------------------------|
| 0 | <i>n</i> | -1.9×10^{12} | 5.2×10^2 | 6.5×10^3 |
| 5 | <i>p</i> | 2.6×10^{12} | 4.8×10^2 | 5.0×10^3 |
| 10 | <i>p</i> | 2.9×10^{12} | 3.9×10^2 | 1.6×10^3 |
| 15 | <i>p</i> | 1.5×10^{13} | 2.7×10^2 | 1.5×10^3 |
| 20 | <i>p</i> | 2.3×10^{13} | 1.3×10^2 | 4.3×10^2 |
| 25 | <i>p</i> | 5.2×10^{14} | 7.8×10^1 | 1.6×10^2 |

conductivity of the thin films was weak, primarily residing in the high-resistance state, characterized by high resistivity and low carrier concentration. However, overall, as the N₂ flow rate increased, the resistivity of the film decreased and the carrier concentration increased. Furthermore, by measuring both positive and negative carrier concentrations, it can be reliably concluded that the intrinsic Ga₂O₃ thin film exhibited n-type conductivity, consistent with other literature reports. When N₂ was introduced for the RF-sputtering growth of the nitrogen-doped Ga₂O₃ thin films, the conductivity became p-type. This verifies that the p-type conductivity of Ga₂O₃ thin films could be achieved through the intentional doping of nitrogen by RF sputtering, and the specific conductivity was closely related to the concentration of nitrogen doping.

For the nitrogen-doped Ga₂O₃ thin films at different N₂ flow rates, MSM-type UV PDs were fabricated. The correlated *I*-*V* characteristics measured at room temperature are shown in Figs. 8(a)–8(d), where Fig. 8(a) represents the dark current. It is evident that with the N₂ flow rate, the electrical conductivity of the devices increased, confirming the effect of nitrogen doping. This trend is consistent with the Hall effect measurements. The N₂ flow rate of the 0 sccm (undoped) sample exhibited extremely high resistance, whereas the nitrogen-doped film and the aluminum electrode formed excellent ohmic contacts, as demonstrated by the linear increase in dark current with the voltage. Figure 8(b) shows the photocurrents measured under deep UV irradiation with a wavelength of 254 nm and a power density of 58 μ W/cm² at 5 V bias. The photocurrent reached 5.1×10^{-8} A for the device corresponding to the 25 sccm N₂ flow rate. Owing to the redshift of the absorption edge caused by nitrogen doping, the optical band gap decreased. Therefore, irradiation and testing were also performed with a longer wavelength of 365 nm near-UV light and a power density of 1.35 mW/cm². The schematic diagram of the measurement under 254 or 365 nm illumination is shown in Fig. 8(c), and Fig. 8(d) shows the *I*-*V* test results under 365 nm illumination. It can be observed that, compared with the results of 254 nm illumination, the photocurrents of the PDs corresponding to the N₂ flow rates of 0 and 5 sccm decreased, whereas those of the PDs corresponding to the N₂ flow rates of 10 and 25 sccm slightly increased, further confirming the effect of nitrogen doping. Under 365 nm illumination, for a PD corresponding to a N₂ flow rate of 25 sccm, its photocurrent of 2.1×10^{-7} A increased more than four times, indicating that the nitrogen-doped Ga₂O₃-based PDs were more sensitive to 365-nm-wavelength UV light.

A PD prepared from nitrogen-doped Ga₂O₃ thin films grown at the N₂ flow rate of 25 sccm underwent an on/off light cycle under a bias voltage of 5 V. The time response characteristics of the device under 365 and 254 nm irradiations were measured, and the *I*-*t* results are shown in

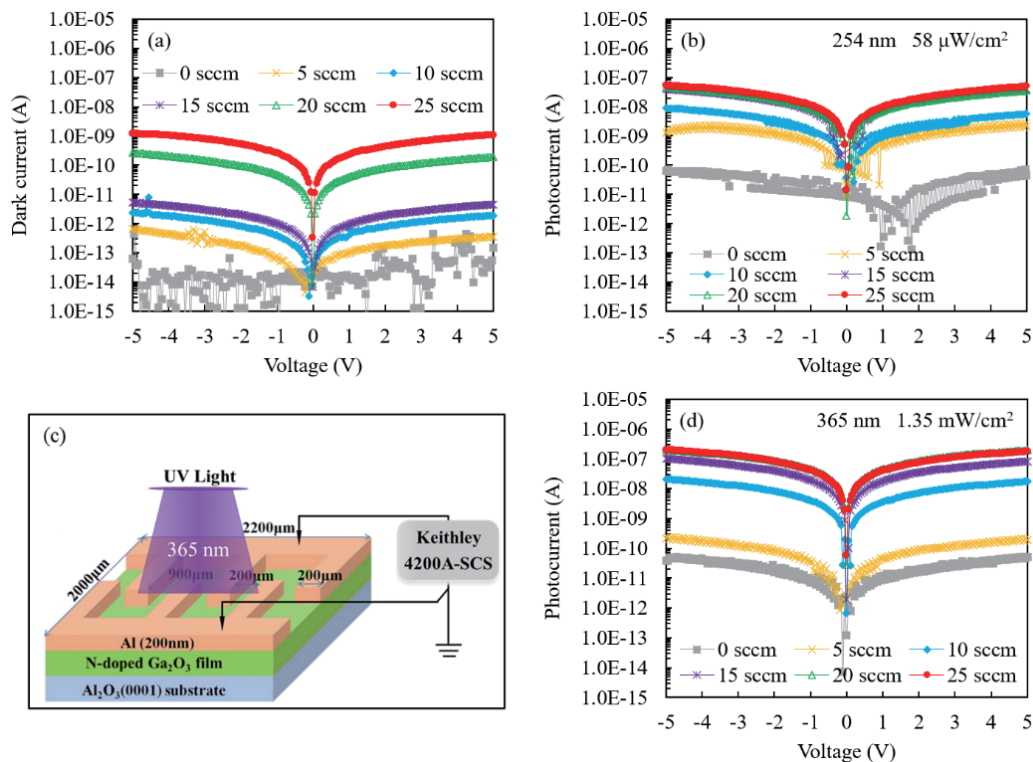


Fig. 8. (Color online) I - V characteristics of nitrogen-doped Ga_2O_3 -based UV PDs under different N_2 flow rates: (a) dark current, (b) photocurrent under 254 nm illumination, (c) measurement schematic diagram under 254 or 365 nm illumination, and (d) photocurrent under 365 nm illumination.

Figs. 9(a)–9(d). Figures 9(a) and 9(b) depict the multicycle I - t characteristic curves measured under 365 nm near-UV light (UV-A) and 254 nm deep UV light (UV-C) irradiations, respectively. After multiple light cycles, the response performance of the detection device remained almost the same, demonstrating excellent repeatability and stability. Under 365 nm UV light irradiation, the current instantly increased by two orders of magnitude. Moreover, under 254 nm UV irradiation, the dark current increased rather slowly from about 1.7×10^{-9} to about 30.7×10^{-9} A. Additionally, it was observed that the recovery times for the rise and fall of I - t curves under 365 or 254 nm UV light were different. For a more detailed comparative study on response time, a quantitative analysis was carried out on the rise and fall of the current, as shown in Figs. 9(c) and 9(d). It was observed that both the rise and fall of the response current under 365 nm illumination were steep, with τ_R and τ_D being 0.028 and 0.17 s, respectively. In contrast, the device exhibited a slow time response when illuminated at 254 nm, with τ_R being 2.95 s, and the photocurrent was unstable, resulting in a slower recovery, with τ_D reaching 9.17 s. This confirms again that nitrogen doping had higher selectivity for long-wavelength UV light. Furthermore, the current drop of the device after UV irradiation did not fully recover to the initial dark current (higher), which was due to defects caused by the lack of crystallization in the thin film, consistent with the XRD results shown in Fig. 6.

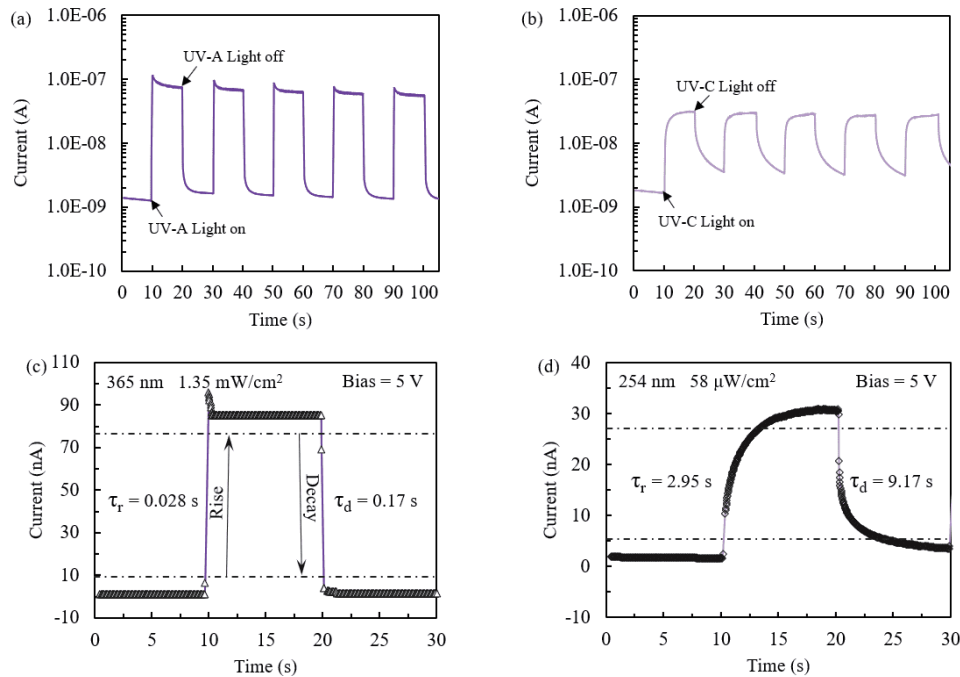


Fig. 9. (Color online) $I-t$ characteristics of nitrogen-doped Ga_2O_3 -based PD at N_2 flow rate of 25 sccm: (a) multiple periods under 365 nm illumination, (b) multiple periods under 254 nm illumination, (c) single period under 365 nm illumination, and (d) single period under 254 nm illumination.

4. Conclusions

In this article, we presented the growth of nitrogen-doped amorphous Ga_2O_3 thin films through reactive sputtering with N_2 gas. A comprehensive investigation was conducted to explore the impact of various N_2 flow rates on the growth rate, morphology, composition, and optical and electrical properties of the thin films. XPS results revealed an increase in the relative content of oxygen defects from 7.06 to 22.21% with the N_2 flow rate. Notably, a flow rate of 20 sccm yielded the smoothest surface morphology. Hall effect testing disclosed that intrinsic Ga_2O_3 thin films exhibited n-type conductivity. However, when N_2 was introduced for sputtering the growth of nitrogen-doped amorphous Ga_2O_3 thin films, the conductivity type shifted to p-type, with the Hall hole concentration increasing proportionally with the N_2 flow rate. Ultimately, MSM-type PDs were fabricated using the nitrogen-doped amorphous Ga_2O_3 thin films. These PDs demonstrated heightened sensitivity to 365 nm near-UV light, boasting a high response of 1.32×10^2 A/W and a rapid response of 0.028/0.17 s.

Acknowledgments

This work was supported by the post-subsidy project for the industry education research of Xiamen Science and Technology Bureau, Fujian Province, China (Grant No. 2023CX0322). We also thank the China Jiangsu 3rd Generation Semiconductor Research Institute Co., Ltd., for its support of the relevant tests conducted in this study.

References

- 1 S. J. Pearton, J. Yang, P. H. Cary, F. Ren, J. Kim, M. J. Tadjer, and M. A. Mastro: *Appl. Phys. Rev.* **5** (2018) 011301.
- 2 J. Zhang, J. Shi, D. C. Qi, L. Chen, and K. H. L. Zhang: *APL Mater.* **8** (2020) 020906.
- 3 M. Higashiwaki, K. Sasaki, A. Kuramata, T. Masui, and S. Yamakoshi: *Appl. Phys. Lett.* **100** (2012) 013504.
- 4 H. Xue, Q. He, G. Jian, S. Long, T. Pang, and M. Liu: *Nanoscale Res. Lett.* **13** (2018) 290.
- 5 H. Zhang, L. Yuan, X. Tang, J. Hu, J. Sun, Y. Zhang, Y. Zhang, and R. Jia: *IEEE Trans. Power Electron.* **35** (2020) 5157.
- 6 Z. Galazka: *Semicond. Sci. Technol.* **33** (2018) 113001.
- 7 D. Guo, Q. Guo, Z. Chen, Z. Wu, P. Li, and W. Tang: *Mater. Today Phys.* **11** (2019) 100157.
- 8 A. Singh Pratiyush, S. Krishnamoorthy, S. Vishnu Solanke, Z. Xia, R. Muralidharan, S. Rajan, and D. N. Nath: *Appl. Phys. Lett.* **110** (2017) 221107.
- 9 E. G. Villora, S. Arjoca, K. Shimamura, D. Inomata, and K. Aoki: *Proc. Oxide-Based Materials and Devices V* **8987** (2014) 371.
- 10 X. Wang, Q. Xu, M. Li, S. Shen, X. Wang, Y. Wang, Z. Feng, J. Shi, H. Han, and C. Li: *Angewandte Chemie.* **124** (2012) 13266.
- 11 G. Eranna, B. C. Joshi, D. P. Runthala, and R. P. Gupta: *Crit. Rev. Solid State Mater. Sci.* **29** (2004) 111.
- 12 M. García-Carrión, J. Ramírez-Castellanos, E. Nogales, B. Méndez, C. C. You, S. Karazhanov, and E. S. Marstein: *Mater. Lett.* **261** (2020) 127088.
- 13 X. Liu, C. Yu, C. Li, and J. Lin: *J. Electrochem. Soc.* **154** (2007) 86.
- 14 Z. Galazka, K. Irmischer, R. Uecker, R. Bertram, M. Pietsch, A. Kwasniewski, M. Naumann, T. Schulz, R. Schewski, D. Klimm, and M. Bickermann: *J. Cryst. Growth* **404** (2014) 184.
- 15 Z. Galazka, R. Uecker, K. Irmischer, M. Albrecht, D. Klimm, M. Pietsch, M. Brützam, R. Bertram, S. Ganschow, and R. Fornari: *Cryst. Res. Technol.* **45** (2010) 1229.
- 16 T. Zhang, Y. Li, Y. Zhang, Q. Feng, J. Ning, C. Zhang, J. Zhang, and Y. Hao: *J. Cryst. Growth.* **859** (2021) 157810.
- 17 Y. Zhang, F. Alema, J. S. Speck, A. Mauze, O. S. Koksaldi, R. Miller, and A. Osinsky: *J. Alloys Compd.* **7** (2019) 022506.
- 18 P. Vogt, F. V. E. Hensling, K. Azizie, C. S. Chang, D. Turner D, J. S. Park, J. P. McCandless, H. J. Paik, B. J. Bocklund, G. Hoffman, O. Bierwagen, D. Jena, H. G. Xing, S. Mou, D. A. Muller, S. L. Shang, Z. K. Liu, and D. G. Schlom: *APL Mater.* **9** (2021) 031101.
- 19 A. Kuramata, K. Koshi, S. Watanabe, Y. Yamaoka, T. Masui, and S. Yamakoshi: *Jpn. J. Appl. Phys.* **55** (2016) 1202A2.
- 20 P. Schurig, M. Couturier, M. Becker, A. Polity, and P. J. Klar: *Physica Status Solidi A* **216** (2019) 1900385.
- 21 Y. Zhang, J. Yan, Q. Li, C. Qu, L. Zhang, and T. Li: *Physica B: Condens. Matter.* **40** (2011) 852.
- 22 V. Patil, B. T. Lee, and S. H. Jeong: *J. Alloys Compd.* **894** (2022) 162551.
- 23 Z. Y. Wu, Z.X. Jiang, C. C. Ma, W. Ruan, Y. Chen, H. Zhang, G. Q. Zhang, Z. L. Fang, J. Y. Kang, and T. Y. Zhang: *Mater. Today Phys.* **17** (2021) 100356.
- 24 Y. Liu, S. Wei, C. Shan, M. Zhao, S. Y. Lien, and M. Lee: *J. Mater. Res. Technol.* **21** (2022) 3113.
- 25 D. Zhang, W. Zheng, R. C. Lin, T. T. Li, Z. J. Zhang, and F. Huang: *J. Alloys Compd.* **735** (2018) 150.